Evaluation of infection risk of two endoparasites to moose (Alces alces) in the Adirondack Park of New York

Alec Wong[1], Krysten Schuler[1], Angela Fuller[1,2,3]

[1]Cornell University
[2]New York Cooperative Fish and Wildlife Research Unit
[3]U.S. Geological Survey

Abstract

Endoparasites *Parelaphastrongylus tenuis* and *Fascioloides magna* were attributed to 19% and 21% of mortalities in New York in 2015, respectively, and may be contributing factors to limiting moose (*Alces alces*) populations in the Adirondacks region. Field surveys were conducted to collect white-tailed deer (*Odocoileus virginianus*) fecal pellets under distance sampling protocol both to measure relative deer density and to diagnose the infection status of the pellets by *P. tenuis* and *F. magna*. Over the three years of data collection, 41.7% of fecal pellets collected ($N = 656$) contained *F. magna* eggs, and 34.7% of fecal pellets contained L1 *P. tenuis* larvae. We attempted to quantify the geospatial distribution of parasite infection using landscape variables such as habitat, geomorphon structure, elevation, and spatial trend, but goodness-of-fit tests indicated poor fit of the model structures we evaluated, whether assessed as continuous intensity of infection (Poisson, negative binomial), or binary infection status (binomial). We conclude that the data are not extensive enough to quantify relationships between parasite infection in white-tailed deer fecal pellets and geospatial effects.

Introduction

Moose (*Alces alces*) populations are in decline in parts of their range in North America such as in Minnesota, Vermont, and New Hampshire in the United States of America and Nova Scotia, Alberta, Saskatchewan, Manitoba, and Ontario in Canada (Lankester 2018; Timmermann and Rodgers 2017). Some researchers point to parasite infection from liver fluke (*Fascioloides magna*) and/or brainworm (*Parelaphastrongylus tenuis*) as contributing factors to these declines (Murray et al. 2006; Lankester 2010, 2018; Wünschmann et al. 2015), although this claim is controversial (Lenarz 2009) and in some areas may coincide with other factors such as depredation or low reproduction rates that may disguise effects of parasite infection (Barber-Meyer and David Mech 2016; Kuzyk et al. 2018). Nevertheless, brain worm and liver fluke cause morbidity and mortality in moose populations and should be monitored.

Infections by *P. tenuis* are benign to white-tailed deer (*Odocoileus virginianus*), but cause severe neurological disorders in moose caused by migration of larvae through the central nervous system that often end in death (Pybus 2001; Lankester 2010). *Parelaphastrongylus tenuis* is acquired via ingestion of gastropod intermediate hosts, in which *P. tenuis* larvae have molt from L1 to L2, and L3 stages over approximately 4 weeks. Gastropods become infected by ingesting the mucosal layer surrounding white-tailed deer fecal pellets, or from the soil over which the L1-stage larvae have been washed by precipitation.

Fascioloides magna infection damage manifests as lesions in the hepatic tissue due to migration of immature flukes or fibrous encapsulation of adult flukes (Pybus 2001). Again, moose are thought to become infected through ingestion of gastropod intermediate hosts. A major distinction is that the gastropod hosts are aquatic snails (typically within the genus *Lymnaea*) that become infected by free-swimming miracidia introduced to the water as eggs in white-tailed deer feces (Pybus 2001; Peterson et al. 2013; Malcicka 2015). The miracidia develop within the snail, ultimately generating cercariae that encyst as metacercariae on aquatic vegetation. Because moose select aquatic vegetation as a significant proportion of their diet, *F. magna* metacercariae are presumably commonly consumed by moose.

In the Adirondacks of New York, moose populations have increased since their extirpation in the late 19th century, but their populations have not seen the same growth during the 20th century as their New England counterparts (Timmermann and Rodgers 2017). Recent estimates of moose population size indicate that there are approximately 600 to 1000 moose in the Adirondacks (Wong, Fuller, and Royle 2018), a range which does not indicate substantial change from previous assertions of population size (Hickey 2008). Factors that may be limiting the population are not established, but the focal parasites *P. tenuis* and *F. magna* have been observed in moose necropsies with moderate frequency.

The New York State Department of Environmental Conservation (DEC) has been gathering information on moose health from incidental mortalities (n = 117) since 2000 and the Animal Health Diagnostic Center (AHDC) started live moose testing in 2015. Moose in New York State appear to be substantially impacted

by several parasites excepting winter ticks, which are more common in New England states. Over 19% of mortalities were attributed to P. tenuis, 21% of moose carcasses examined were infected with liver flukes (Fascioloides magna). Migrating parasites cannot be detected in live moose, but were likely a problem as New York moose had 5-6x higher eosinophil (white blood cell) counts than New Hampshire or Maine moose.

The geospatial distribution of infection risk to moose is a concern for management, and we attempt to quantify this by first assessing the spatial patterns in infection of white-tailed deer fecal matter.

Materials and Methods

Study area

We surveyed within the Adirondack Park of the state of New York. It is an area of approximately 24,000 km^2, composing approximately 17% of the state of New York. Elevation ranges from 100m - 1600m. The Adirondack Park contains primarily upland forest habitat dominated by such species as American beech (*Fagus grandifolia*), red spruce (*Picea rubens*), hemlock (*Tsuga canadensis*), sugar maple (*Acer saccharum*), striped maple (*Acer pensylvanicum*), and balsam fir (*Abies balsamea*). Approximately 20% of the park is composed of wetland habitats including open river corridors, floating bogs, and large open bogs dominated by conifers (Hickey 2008).

Field data collection

White-tailed deer fecal pellet groups were collected opportunistically during the years of 2016 and 2017 for the purpose of parasite quantification during a larger survey investigating the population size of moose in the park. The moose study surveyed triangular transects approximately 3 km long, selected by cluster random sampling. The clustering design of the transects were optimized for a spatial capture-recapture survey, including 3 transects per cluster separated by approximately 2-4 km.

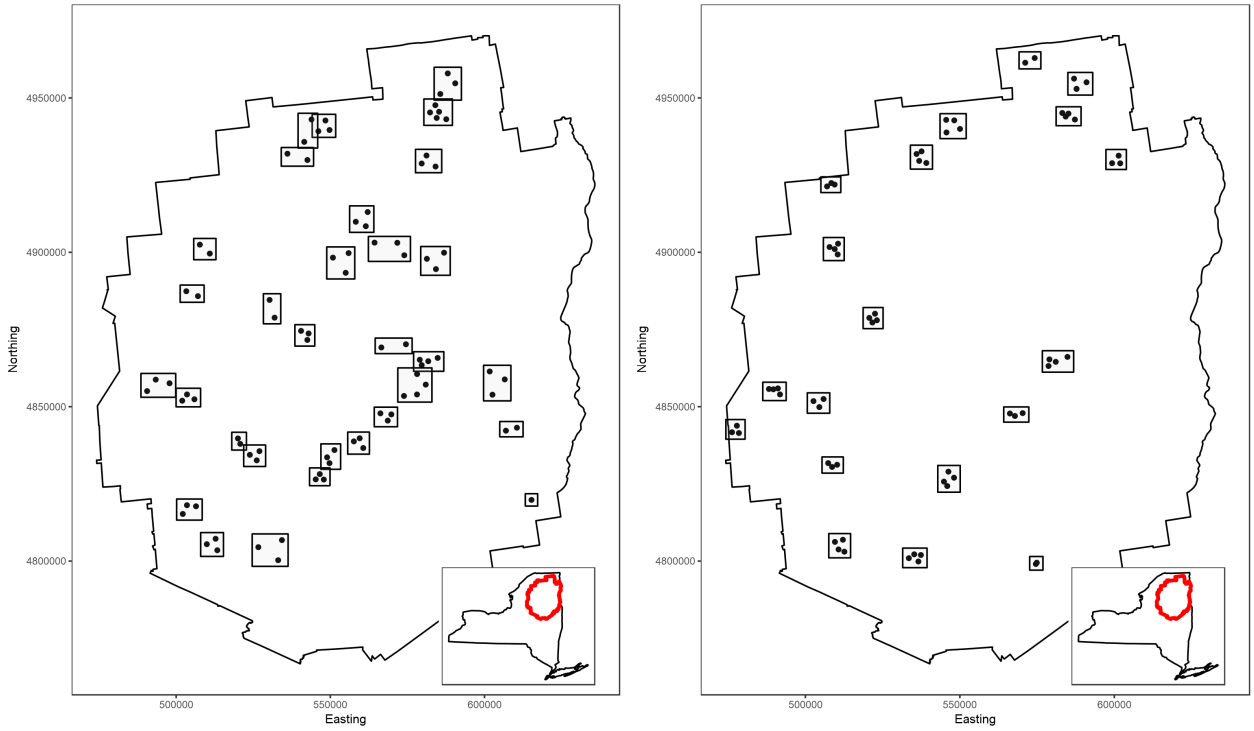

(a) Transect locations within the Adirondack Park for the 2016 survey.

(b) Transect locations within the Adirondack Park for the 2017 survey.

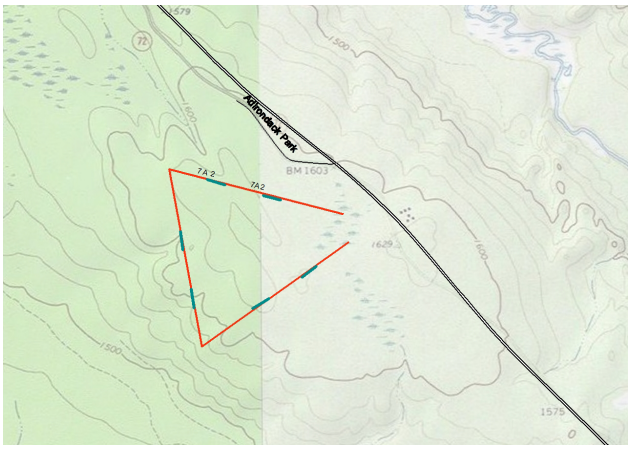

(c) Example of a parent 'moose' transect (red) approximately 3 km in length. It contains six child 'deer' transects (turquoise) that are each 100m in length and separated by 200m at a minimum.

Figure 1: Transect locations within the Adirondack Park each year of surveys. In figures (a) and (b), each dot represents the location of one transect, and each cluster of transects is bounded by a box. The inlaid plot indicates the extent of the Adirondack Park relative to the state of New York. Figure (c) depicts the typical transect design.

In 2018, a single-observer distance sampling protocol was implemented intended to quantify deer fecal group abundance in addition to measuring parasite intensity. Along each moose transect, 6 distance sampling transects each 100m long were spaced 200m apart from each other (Figure 1c).

A total of 150 such sub-transects were sampled in 2018. At the specified start point, field technicians extended

a 100m tape to serve as the center line, and made observations along its length. Any number of scat pellets were considered to constitute a fecal group, and the approximate number was recorded. When a fecal group was detected, its distance perpendicular from the center line, and parallel along the center line was recorded. The perpendicular distance is the focal variable of distance sampling, but the parallel distance provided highly precise location coordinates of the scats – because the start point of the transect was recorded with greater accuracy (due to longer GPS averaging time), the coordinates of the scats could be refined by translating the start point in space by the angle of the transect, and the parallel distance away from the start point.

Fifty-seven white-tailed deer fecal samples were collected in 2016, 391 samples were collected in 2017, and 174 samples were collected in 2018.

Parasitological analyses

The fecal samples were analyzed by the Cornell Animal Health and Diagnostic Center using several methods. For *F. magna*, Flukefinder, a modified Baermann technique, and fecal quantitative flotation were used. For *P. tenuis*, the modified Baermann, and fecal quantitative flotation methods were implemented. After 2016, the diagnostic method for *F. magna* used was Flukefinder, and for *P. tenuis*, the modified Baermann technique.

Flukefinder

Needs to be updated by relevant members

Modified Baermann

Needs to be updated by relevant members

Fecal flotation

Needs to be updated by relevant members

Statistical Models

For analysis of relative risk of infection to moose, we implemented a hierarchical Bayesian modeling framework analyzed with the `R` package `INLA`, which uses integrated nested Laplace approximation to approximate the posterior distribution of model parameters.

Parasite intensity model

Let $\widehat{\lambda}(s)$ be the estimated per-fecal-group-sample abundance (or, intensity in the epidemiological sense). Let $S = \{s_i, i = 1, ..., n\} \subset \Omega$ be the n distinct locations where white-tailed deer fecal groups were observed within the observation region $\Omega \subseteq \mathbb{R}^2$, and let y_i be the observed parasite count within the fecal sample.

Parasites observed within each scat sample are ≥ 0, and due to the high prevalence of 0's, we considered a negative binomial distribution for the response in addition to the Poisson. On any bounded region $B \subseteq \Omega$, observations are thus modeled as follows:

$$\begin{gathered} y_i \sim \text{Poisson}(\mu_i) \\ \log(\mu_i) = \beta_0 + \beta_1 * x_1(s_i) + ... + \beta_p * x_p(s_i) + \Psi(s_i) \\ \Psi(s_i) \sim GP(0, \Sigma) \end{gathered} \tag{1}$$

Where, y_i represent the parasites observed per fecal group sample, μ_i is the mean function modeled dependent upon spatial covariates $x_j(s)$, and $\Psi(s)$ is a Gaussian process with mean 0 and covariance matrix Σ. The covariance function used is the Matern; with $\nu = \alpha - d/2$, and $\alpha = 2; d = 2$:

$$\text{cov}[\Psi(s), \Psi(s')] = \sigma^2 \ \kappa||s' - s|| \ \mathcal{K}_1(\kappa||s' - s||)$$

where κ is the Matern spatial scale parameter such that $\kappa = \sqrt{8\nu}/\rho$. The marginal variance is $\sigma^2 = 1/(4\pi\kappa^2\tau^2)$, where τ is the precision. $\mathcal{K}_1$ is the modified Bessel function of the second kind and order 1 (Lindgren and Rue 2015).

We selected this error model to account for the fact that the spatially clustered sampling is likely to obtain multiple samples from the same individuals, inducing local spatial autocorrelation. While empirical variograms do not suggest autocorrelation at any distance for *F. magna* response values, there exists observed autocorrelation for *P. tenuis* at the scale of approximately 1200 m.

Additionally, we assessed the fit of models treating the response as a binary random variable modeled under the binomial distribution and zero-inflated binomial distribution, with the same model of spatial dependence instead using the appropriate link function.

Covariates on parasite intensity

In our model, we consider the following covariate effects on parasite intensity. Coordinate data (UTM Easting and Northing) are included to model broad-scale spatial trend. We considered a derived variable of precipitation representing the total accumulation of precipitation in the year prior to the data collection date, measured in inches. Precipitation affects the survival of *P. tenuis* and *F. magna* outside of a host (i.e. as L1 larvae, and eggs in feces, respectively), and so it is anticipated that deer would be more likely to be infected in areas of higher rainfall (Pybus 2001). Additionally, gastropod activity is inhibited by drought, and so higher rainfall would suggest higher risk of infection due to a greater availability of gastropods to be ingested in the case of *P. tenuis* (Lankester 2018). We used the spatially interpolated PRISM dataset for precipitation (PRISM Climate Group 2019). We considered another derived variable for snowfall accumulation in the snowfall season prior to the data collection date (that is, from September until April in the year prior to the date of survey). Similar to precipitation, we anticipate that areas that experience low snowfall in the year prior to the survey date will exhibit a higher parasite intensity due to increased parasite survival, and increased activity of gastropod intermediate hosts. The National Weather Service's National Snowfall Analysis (2019) dataset was used to obtain spatially-referenced snowfall amounts.

Local terrain basins where water may collect were considered as a potentially important effect particularly for *F. magna*, as the life cycle of the parasite has a period during which metacercariae encyst on aquatic vegetation and once matured infect aquatic snail intermediate hosts. We hypothesized that intensity of infection for *F. magna* will be greater in basins than on slopes or peaks, and we assessed this by the geomorphon tool in QGIS, assessed at a range of 40km (1600 squared-kilometers). This range was selected because it maximized the variation in the geomorphon classification distribution relative to our sample locations.

INLA settings

Priors

We used default priors set by INLA for the covariate coefficients; that is:

$$\beta_p \sim \text{Normal}(0, 0.001)$$

where the second argument of the Normal distribution is specified on the *precision* scale.

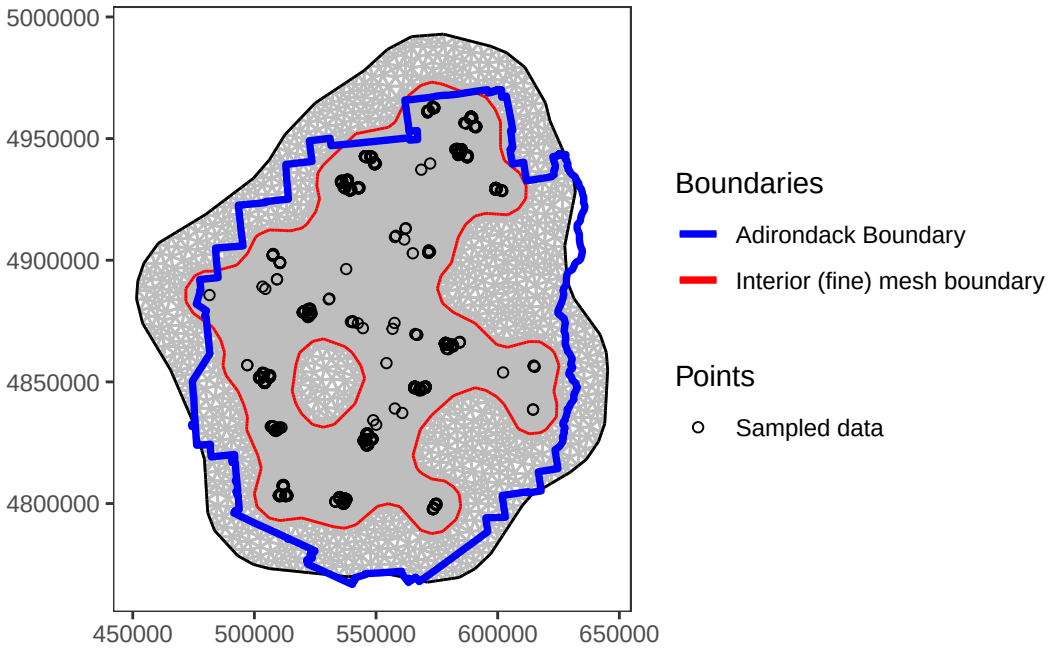

Figure 2: Boundary line of the Adirondack Park (blue), and the mesh constructed for INLA (red).

The priors for the Matern covariance parameters were specified using INLA's penalized complexity prior construction for the spatial range parameter ρ and marginal standard deviation σ_0. The joint density of the prior is:

$$
\begin{aligned}
p(\rho, \sigma_0) &= \frac{(d * R * S)}{2} \rho^{-1-\frac{d}{2}} \exp(-R\rho^{\frac{-d}{2}}) \exp(-S\sigma_0) \\
R &= -\log(p_\rho)\rho_0^{\frac{d}{2}} \\
S &= -\frac{\log(p_\sigma)}{\sigma_0}
\end{aligned}
\tag{2}
$$

Critically, p_ρ and p_σ are defined such that:

$$
\begin{aligned}
p_\rho &= P(\rho < \rho_0) \\
p_\sigma &= P(\sigma > \sigma_0)
\end{aligned}
$$

In so doing, the prior specification can be defined on intuitive scales, setting a lower and upper limit for ρ and σ_0, respectively. We selected $\rho_0 = 100$ (meters) and $\sigma_0 = 35$, and $p_\rho = p_\sigma = 0.01$ reasoning that at our scale of inference, spatial autocorrelation < 100m is not substantially different from *i.i.d.* normal error, and the marginal standard deviation would not be much larger than the sample standard deviation.

Mesh

A mesh is required to fit Gaussian random effect models under the INLA framework. The `meshbuilder` tool provided by package `INLA` was used to visually select settings that fulfilled the following criteria (see Figure 2):

- Relatively fine mesh resolution ($<$ 2km edges, $\sim$ 1 km between vertices) in the vicinity of sampled data
- Relatively low mesh resolution far from sampled data (>5km)

Model Specifications

Six models were applied using the covariates developed above upon response variables for both *F. magna* and *P. tenuis*.

Table 1: Model specifications and their covariates

Model	Formula
Null Model	.
Full Model	Easting + Northing + Precipitation + Snow + Geomorphon + Elevation + Gaussian Process (GP)
Fixed Effects Model	Easting + Northing + Precipitation + Snow + Geomorphon + Elevation
Fixed Effects Parasite Survival Model	Precipitation + Snow + Geomorphon
Two-scale spatial model	Easting + Northing + GP
Two-scale spatial model and elevation	Easting + Northing + Elevation + GP

Results

We observed 41.7% positive diagnoses of *F. magna* over the three years of data collection ($N = 656$), with yearly positive results being 69% in 2016, ($N = 80$), 37.8% in 2017 ($N = 402$), and 38.5% in 2018 ($N = 174$). For *P. tenuis* we observed 34.6% infection prevalence among the fecal samples tested over all three years, with yearly positive results being 48.8% in 2016 ($N = 80$), 23.9% in 2017 ($N = 402$), and 52.6% in 2018 ($N = 174$) (Table 2).

Table 2: Raw frequencies and proportions of diagnoses performed on white-tailed deer fecal samples between 2016 and 2018.

		Counts			Proportions		
Diagnosis	Species	2016	2017	2018	2016	2017	2018
Positive	F. magna	55	152	67	0.688	0.378	0.385
	P. tenuis	39	95	92	0.488	0.239	0.526
Negative	F. magna	25	250	107	0.312	0.622	0.615
	P. tenuis	41	302	83	0.512	0.761	0.474

Model results

Model comparison was implemented by comparison of WAIC values produced by INLA. This information criterion is a measure of *relative* out-of-sample predictive accuracy, and lower WAIC values indicate greater relative performance.

Model results for the Poisson response distribution are not included in the table because all WAIC values are an order of magnitude larger than those of the negative-binomial response distribution.

Among the models fit to the *F. magna* data, the best-supported model was the global model, followed by the second-best model with a delta-WAIC value of 24.41.

Among the models fit to the *P. tenuis* data, the best-supported model was the reduced 'two-scale spatial model', which had only easting, northing, and the Gaussian process error model. The next best performing model followed with a delta-WAIC value of 7.06.

Table 3: *F. magna* model WAIC values

Model Name	WAIC
Full model	3052.46
Two-scale spatial model	3076.87
Two-scale spatial model and elevation	3081.90
Fixed effects model	3108.38
Fixed Effects Parasite Survival Model	3110.83
Null Model	3130.45

Table 4: *P. tenuis* model WAIC values.

Model Name	WAIC
Two-scale spatial model	2756.66
Full model	2763.73
Two-scale spatial model and elevation	2767.49
Fixed effects model	2795.65
Fixed Effects Parasite Survival Model	2823.91
Null Model	2824.85

All (and particularly the best-supported) models for the *F. magna* data suggest positive relationships with rainfall and negative relationships with snowfall, in agreement with our hypotheses (Figure 3). For the *P. tenuis* data, there were no comparable relationships with snowfall and precipitation. Elevation presented a strong negative correlation in all models in which it was included, including the model with the highest support.

While most of the geomorphon predictor coefficient estimates had wide posterior distributions overlapping 0 or were estimated to be nearly 0, the geomorphon types that represent sloping features with no flat areas (spur, ridge, hollow) displayed positive effects for both species. Our hypothesis suggested that valleys would exhibit a positive relationship with parasite intensity, but the effects were estimated to be nearly zero with wide posterior distributions. Indeed, ridges (the opposite of valleys) presented a slightly positive association with parasite intensity for both species.

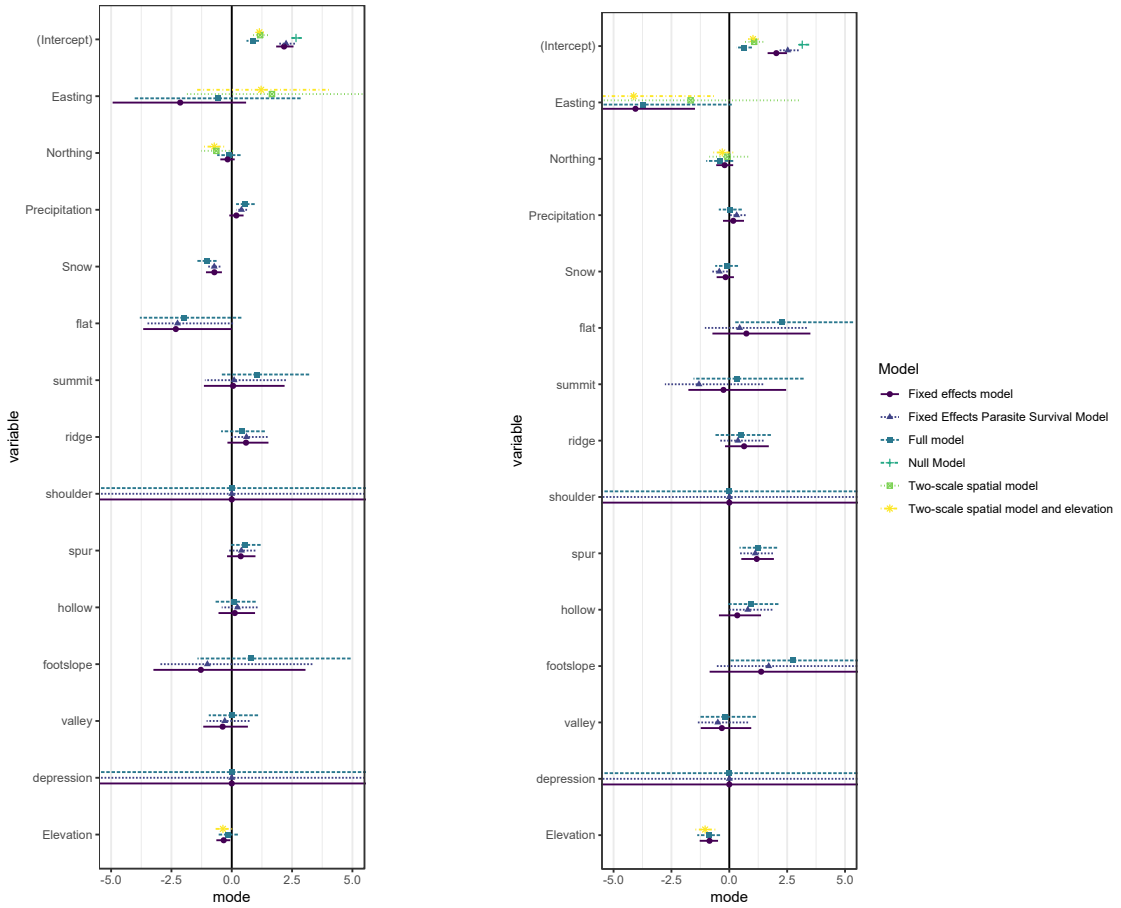

(a) *F. magna* model parameter estimates.

(b) *P. tenuis* model parameter estimates.

Figure 3: Displayed are the mode and 95% credible interval for coefficients of fixed effects. See Appendix A for exact values.

The scale parameter for the random effect varied greatly between models, but the best-supported model for *F. magna* suggest a range of autocorrelation on the order of one kilometer (95% CI 174m - 1690m). For *P. tenuis*, the range parameter varied from 2871 to 19903 with a mean value of 8705 in the best-fitting model.

Bayesian model checks

We checked the fit of the models using Bayesian predictive checks available in the `INLA` package; specifically the conditional predictive ordinate (CPO) and the probability integral transform (PIT).

Conditional predictive ordinate

The conditional predictive ordinate (CPO) is a leave-one-out cross-validation measure, defined as

$$\text{CPO}_i = \pi(y_i^{\text{obs}} | y_{-i})$$

and describes the probability of a particular observation i when all of the data but observation i are used to fit to the model. Very small values indicate that the model is not likely to have predicted a particular observation and thus that model is not expected to generalize well.

All of our models exhibited poor performance with roughly half of the data points having low CPO values less than 0.1 (Figure 4). In addition, the data points with low CPO values are strongly related to those points with the response > 0 (Figure 5). This indicates that the models overall fit the data poorly, having almost no predictive power to the domain of the response of interest.

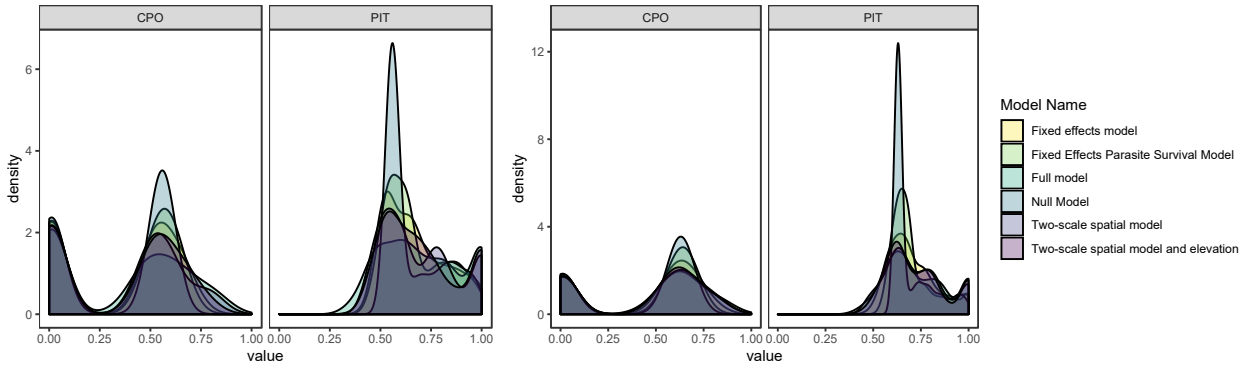

(a) *F. magna* model goodness-of-fit statistics.

(b) *P. tenuis* model goodness-of-fit statistics.

Figure 4: Displayed are the densities of two goodness-of-fit statistics for the models applied to the two parasite species' data. Under good model fit, the CPO values should not have many values approaching zero; the PIT values should be uniformly distributed.

Probability integral transform

Another goodness-of-fit measure that `INLA` provides is the probability integral transform value (PIT), which measures the probability of predicting a new observation less than or equal to the observed data value. More generally the probability integral transform states that the cumulative distribution function $\mathcal{F}$ of a random variable X evaluated at x_i for all i will have a random uniform distribution if the random values x_i are indeed generated by the same process as X. If we take $\mathcal{F}(X)$ to be predictions from a fitted model, departure from uniformity indicates that the observations x_i may not be well predicted by the model.

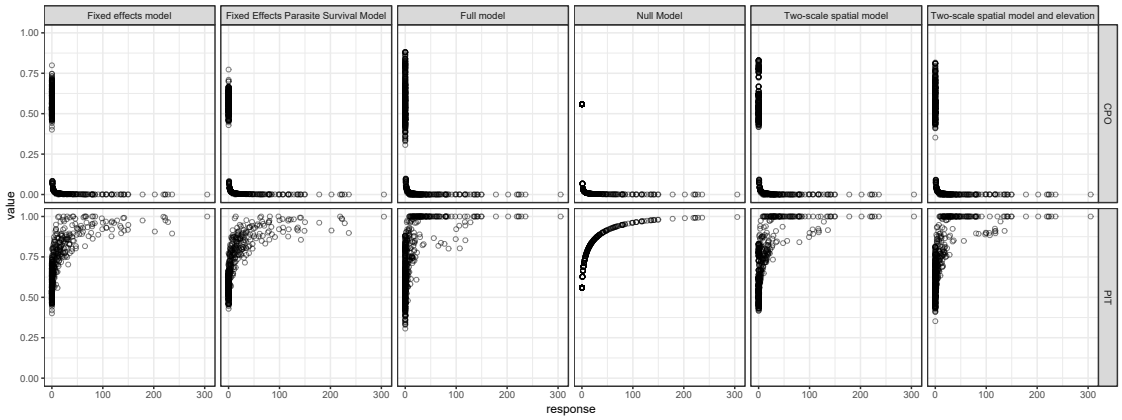

(a) *F. magna* model goodness-of-fit statistics.

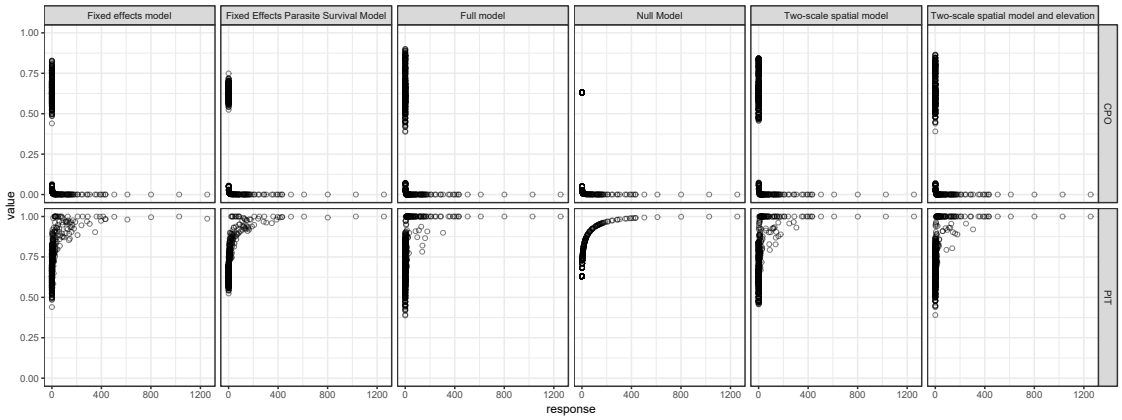

(b) *P. tenuis* model goodness-of-fit statistics.

Figure 5: Displayed are the conditional predictive ordinate and probability transform values across values of the response variable. The goodness-of-fit values are relatively poor when the response is not zero.

By visual assessment, the PIT values are not uniformly distributed (Figure 4), and become more concentrated around 1 with increasing values of the response (Figure 5).

Binary model results

Due to the poor fit, the models were reassessed with the data converted to binary presence-absence data, and the best-performing models by WAIC were re-assessed. The conditional predictive ordinate values were improved, having few values below 0.1. However, the probability integral transform continued to indicate a lack of fit, having a high density of values approaching unity.

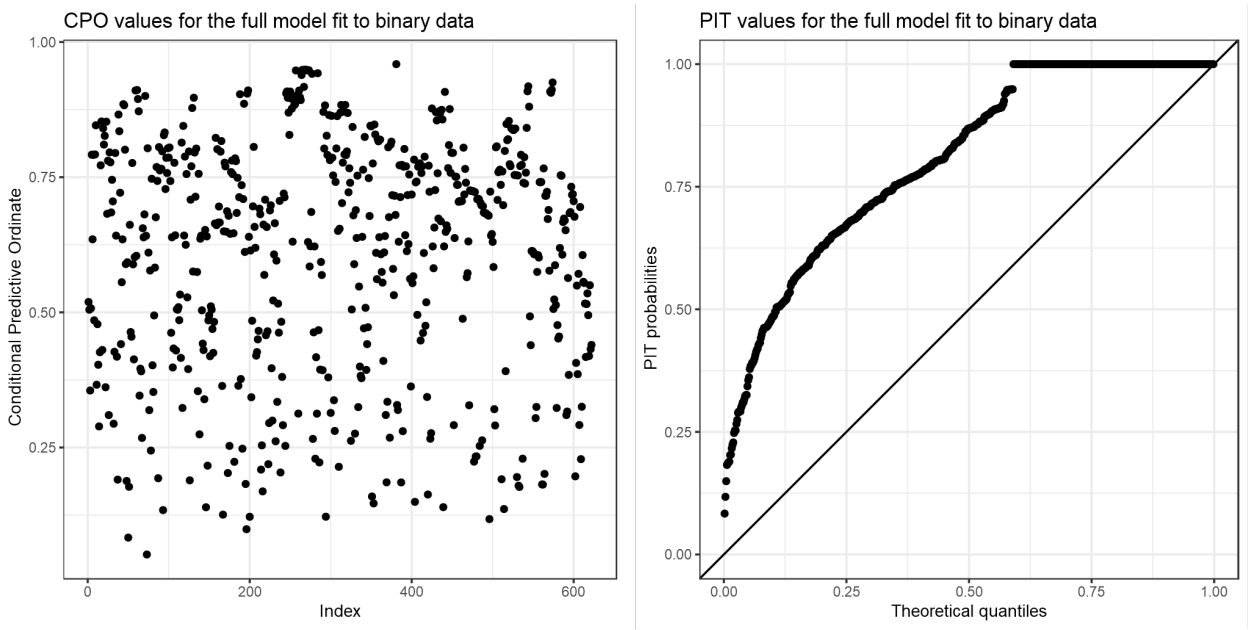

(a) (b)

Figure 6: Displayed are the (a) conditional predictive ordinate and (b) probability transform values quantile-quantile plot for the global model fit to the *F. magna* data. The properties of these goodness-of-fit tests are identical for the *P. tenuis* data.

Discussion

The endoparasites *F. magna* and *P. tenuis* are moderately prevalent in the Adirondack white-tailed deer population, having infected approximately four-in-ten of the deer pellet groups assessed. This is not a direct assessment of the prevalence in white-tailed deer, as it is possible that we sampled multiple pellet groups from the same animal; nevertheless, we anticipate that a relatively greater abundance of infected pellet groups will present a higher risk of infection to gastropod intermediate hosts, though we were unable to quantify the relative spatial risk of infection.

All *F. magna* models including prior-year snowfall and prior-year precipitation as a covariate demonstrate a negative relationship with snowfall and a positive relationship with rainfall, and were among the effects estimated with greatest precision. This is supports the hypothesis that survival of the parasites in the infective stage is a crucial factor in the eventual discharge of more infective stage parasite organisms in the next year.

The *P. tenuis* models did not display as strong a relationship with meteorological factors, indicating that perhaps the liver fluke are more sensitive to weather than are *P. tenuis* infective stages. Since *F. magna* requires additional stages of development in aquatic environments (and thus depending upon distinct species of intermediate hosts), these results are sensible; particularly a greater reliance upon rainfall. Brainworm larvae instead were observed to have a negative relationship with elevation, which may indicate an underlying relationship with habitat, as the habitat transitions to upland coniferous habitat with increasing altitude.

The geomorphon landscape structures were included in the model to quantify whether localized basins where water might collect may be important in determining parasite intensity. Our hypothesis was that lower areas (valleys, depressions) would contribute to greater success of the parasites due to formation of ephemeral water bodies. However, the valley geomorphon exhibited a small *negative* effect, or no effect at all. Instead, areas with sloping characteristics and no flat components (ridge, spur, and hollow) demonstrated positive effects. This suggests that perhaps ephemeral water bodies are not measurably important factors in the distribution of the parasites, and is in contrast to results of previous research (Vanderwaal et al. 2014).

However, it is more likely that our analysis suffered from a lack of data to adequately characterize the relationships. The majority of the data (42.8%, $n = 266$) occurred on slope gemorphons, followed by spur (24.9% $n = 155$), hollow (10.9% $n = 68$), and ridge (10.3%, $n = 64$); in contrast, only 45 observations (7.2%) occurred in valley and 24 observations in any other geomorphon type (3.9%).

Additionally, our analysis of factors explaining the spatial distribution of the parasites are likely inconclusive due to poor model fit. Two goodness-of-fit measures indicate that all model constructions have poor fit, particularly for response values greater than zero. This indicates two things: (a) the selection of the random field parameters are not contributing to the lack of fit (as the models without local spatial effects exhibit the same fit statistics), and (b) the model does not explain the parasite presence very well at all. While the negative binomial model presents a tremendous improvement over the Poisson (with WAIC value improving by an order of magnitude), the overall lack of fit indicates that a different analytical framework is required.

The poor fit persisted when the data were reduced to presence/absence binary information. While the conditional predictive ordinate (CPO) diagnostic plots displayed a low density of small values, a marked improvement, it measures the probability of observing y_i under a model fit to y_{-i} (all data but observation i). Because there are only two possible outcomes (and thus only one way to be wrong) the CPO values may not be as sensitive to poor fit as the probability integral transform (PIT). Under good model fit, PIT values should be uniformly distributed; however, we observed an increasing density of values as they approached 1, and were certainly not uniformly distributed as Figure 6 demonstrates.

We conclude that the spatial covariates included are likely not adequate in explaining the variation in the data, and the number of observations is too sparse to detect a signal over as large a space as the Adirondacks. Future research should devote a more dedicated sampling effort than we could allocate, expanding the spatial extent of sampling and using a sampling design specific to this research question. For instance, sample locations could be selected to maximize covariate variation, where we could not do so due to the constraints of sampling opportunistically within another research context.

References

Barber-Meyer, Shannon, and L. David Mech. 2016. "White-tailed Deer (Odocoileus virginianus) Subsidize Gray Wolves (Canis lupus) During a Moose (Alces americanus) Decline: A Case of Apparent Competition?" *Canadian Field-Naturalist* 130 (4): 308–14. https://doi.org/10.1016/j.tig.2014.09.010.

Hickey, Lisa. 2008. "Assessing re-colonization of moose in New York with HSI models." *Alces* 44 (44): 117–26.

Kuzyk, Gerald, Ian Hatter, Shelley Marshall, Chris Procter, Becky Cadsand, Daniel Lirette, Heidi Schindler, et al. 2018. "Moose Population Dynamics During 20 Years of Declining Harvest in British Columbia." *Alces* 54: 101–19.

Lankester, Murray W. 2018. "Considering weather-enhanced transmission of meningeal worm, Parelaphostrongylus tenuis, and moose declines." *Alces: A Journal Devoted to the Biology and Management of Moose* 54: 1–13. http://alcesjournal.org/index.php/alces/article/view/201.

Lankester, Murray W. 2010. "Understanding the impact of meningeal worm, Parelaphostrongylus tenuis, on moose populations." *Alces* 46: 53–70.

Lenarz, Mark S. 2009. "A review of the ecology of Paralephostrongylus tenuis in relation to deer and moose in North America." *Summaries of Wildlife Research Findings*, no. Benson 1958: 1–7.

Lindgren, Finn, and Håvard Rue. 2015. "Bayesian Spatial Modelling with R - INLA." *Journal of Statistical Software* 63 (19). https://doi.org/10.18637/jss.v063.i19.

Malcicka, Miriama. 2015. "Life history and biology of fascioloides magna (Trematoda) and its native and exotic hosts." *Ecology and Evolution* 5 (7): 1381–97. https://doi.org/10.1002/ece3.1414.

Murray, Dennis L, Eric W Cox, Warren B Ballard, Heather A Whitlaw, Mark S Lenarz, Thomas W Custer, Terri Barnett, and Todd K Fuller. 2006. "Pathogens, nutritional deficiency, and climate influences on

a declining moose population." *Wildlife Monographs* 166 (Murray): 1–30. https://doi.org/10.2193/0084-0173(2006)166[1:PNDACI]2.0.CO;2.

Peterson, William J., Murray W. Lankester, John G. Kie, and R. Terry Bowyer. 2013. "Geospatial analysis of giant liver flukes among moose: Effects of white-tailed deer." *Acta Theriologica* 58 (4): 359–65. https://doi.org/10.1007/s13364-013-0130-4.

PRISM Climate Group. 2019. Oregon State University; http://prism.oregonstate.edu.

Pybus, Margo. 2001. *Parasitic Diseases of Wild Mammals*. Edited by William M. Samuel, Margo J. Pybus, and A. Alan Kocan. Ames, Iowa: Iowa State University Press. https://doi.org/10.2307/1295958.

Timmermann, H R, and Arthur R Rodgers. 2017. "The status and management of moose in North America - Circa 2015." *Alces* 53: 1–22.

Vanderwaal, Kimberly L., Steve K. Windels, Bryce T. Olson, J. Trevor Vannatta, and Ron Moen. 2014. "Landscape influence on spatial patterns of meningeal worm and liver fluke infection in white-tailed deer." *Parasitology* 142 (05): 706–18. https://doi.org/10.1017/S0031182014001802.

Wong, Alec, Angela Fuller, and J. Andrew Royle. 2018. "Methodologies for Abundance Estimation of Moose (Alces Alces) and Other Rare Species." Master's thesis, Cornell University. https://doi.org/10.7298/6adv-ae33.

Wünschmann, Arno, Anibal G. Armien, Erika Butler, Mike Schrage, Bert Stromberg, Jeff B. Bender, Anna M. Firshman, and Michelle Carstensen. 2015. "Necropsy findings in 62 opportunistically collected free-ranging moose (Alces alces) from Minnesota, USA (2003–13)." *Journal of Wildlife Diseases* 51 (1): 157–65. https://doi.org/10.7589/2014-02-037.

2019. National Oceanic and Atmospheric Administration; National Weather Service; https://www.nohrsc.noaa.gov/snowfall_v2/.

Appendices

Appendix A: Parameter estimates for the negative binomial model

Table 5: Fixed effect parameter estimates and distribution for *F. magna*

variable	mean	sd	0.025quant	0.5quant	0.975quant	mode
Null Model						
(Intercept)	2.670	0.116	2.450	2.668	2.905	2.663
Full model						
(Intercept)	0.871	0.132	0.610	0.871	1.129	0.872
Easting	-0.573	1.750	-4.028	-0.568	2.854	-0.559
Northing	-0.122	0.247	-0.604	-0.123	0.367	-0.125
Precipitation	0.560	0.197	0.179	0.559	0.952	0.555
Snow	-1.036	0.214	-1.470	-1.031	-0.628	-1.022
flat	-1.832	1.071	-3.811	-1.877	0.399	-1.970
summit	1.217	0.930	-0.444	1.158	3.209	1.036
ridge	0.442	0.463	-0.445	0.434	1.373	0.419
shoulder	0.000	31.623	-62.086	-0.001	62.034	0.000
spur	0.551	0.326	-0.083	0.548	1.197	0.544
hollow	0.136	0.423	-0.671	0.128	0.993	0.111
footslope	1.325	1.625	-1.423	1.164	4.928	0.817
valley	0.035	0.520	-0.954	0.023	1.091	0.000
depression	0.000	31.623	-62.086	-0.001	62.034	0.000

Table 5: Fixed effect parameter estimates and distribution for *F. magna (continued)*

variable	mean	sd	0.025quant	0.5quant	0.975quant	mode
Elevation	-0.161	0.213	-0.585	-0.160	0.254	-0.157
Two-scale spatial model						
(Intercept)	1.184	0.153	0.888	1.181	1.500	1.175
Easting	1.701	1.856	-1.962	1.690	5.416	1.666
Northing	-0.626	0.331	-1.271	-0.631	0.054	-0.639
Two-scale spatial model and elevation						
(Intercept)	1.140	0.101	0.938	1.141	1.335	1.145
Easting	1.249	1.402	-1.483	1.239	4.030	1.217
Northing	-0.733	0.215	-1.165	-0.731	-0.315	-0.725
Elevation	-0.368	0.198	-0.762	-0.367	0.019	-0.366
Fixed effects model						
(Intercept)	2.184	0.183	1.840	2.178	2.559	2.167
Easting	-2.154	1.408	-4.938	-2.148	0.594	-2.137
Northing	-0.173	0.152	-0.473	-0.173	0.123	-0.172
Precipitation	0.191	0.151	-0.102	0.191	0.489	0.189
Snow	-0.730	0.168	-1.069	-0.727	-0.408	-0.721
flat	-2.058	0.936	-3.670	-2.142	0.000	-2.318
summit	0.305	0.854	-1.154	0.225	2.189	0.055
ridge	0.632	0.432	-0.180	0.618	1.521	0.591
shoulder	0.000	31.623	-62.086	-0.001	62.034	0.000
spur	0.383	0.300	-0.194	0.379	0.983	0.371
hollow	0.168	0.385	-0.549	0.153	0.965	0.125
footslope	-0.618	1.619	-3.247	-0.821	3.056	-1.281
valley	-0.315	0.471	-1.181	-0.336	0.669	-0.379
depression	0.000	31.623	-62.086	-0.001	62.034	0.000
Elevation	-0.343	0.147	-0.639	-0.340	-0.062	-0.335
Fixed Effects Parasite Survival Model						
(Intercept)	2.267	0.172	1.945	2.262	2.620	2.251
Precipitation	0.406	0.114	0.186	0.404	0.634	0.402
Snow	-0.733	0.137	-1.008	-0.730	-0.470	-0.726
flat	-1.980	0.922	-3.558	-2.066	0.054	-2.248
summit	0.349	0.858	-1.115	0.268	2.244	0.096
ridge	0.656	0.400	-0.087	0.640	1.487	0.609
shoulder	0.000	31.623	-62.086	-0.001	62.034	0.000
spur	0.410	0.285	-0.137	0.406	0.980	0.398
hollow	0.284	0.378	-0.417	0.269	1.070	0.239
footslope	-0.340	1.622	-2.969	-0.545	3.342	-1.011
valley	-0.218	0.453	-1.043	-0.242	0.738	-0.289
depression	0.000	31.623	-62.086	-0.001	62.034	0.000

Table 6: Fixed effect parameter estimates and distribution for *P. tenuis*

variable	mean	sd	0.025quant	0.5quant	0.975quant	mode
Null Model						
(Intercept)	3.163	0.141	2.897	3.160	3.452	3.152
Full model						
(Intercept)	0.646	0.173	0.299	0.649	0.978	0.656

Table 6: Fixed effect parameter estimates and distribution for *P. tenuis (continued)*

variable	mean	sd	0.025quant	0.5quant	0.975quant	mode
Easting	-3.802	2.021	-7.848	-3.778	0.110	-3.732
Northing	-0.413	0.297	-0.999	-0.413	0.170	-0.412
Precipitation	0.032	0.254	-0.455	0.028	0.541	0.021
Snow	-0.100	0.251	-0.610	-0.094	0.377	-0.082
flat	2.542	1.309	0.219	2.453	5.349	2.267
summit	0.596	1.212	-1.548	0.510	3.212	0.332
ridge	0.544	0.622	-0.649	0.534	1.798	0.514
shoulder	0.000	31.623	-62.086	-0.001	62.034	0.000
spur	1.247	0.415	0.439	1.244	2.067	1.239
hollow	0.996	0.556	-0.060	0.984	2.124	0.959
footslope	3.462	2.058	0.041	3.239	8.063	2.747
valley	-0.134	0.629	-1.322	-0.151	1.151	-0.184
depression	0.000	31.623	-62.086	-0.001	62.034	0.000
Elevation	-0.891	0.251	-1.385	-0.892	-0.398	-0.892
Two-scale spatial model						
(Intercept)	1.073	0.200	0.673	1.073	1.468	1.074
Easting	-1.684	2.378	-6.408	-1.679	3.002	-1.671
Northing	-0.053	0.423	-0.862	-0.063	0.816	-0.082
Two-scale spatial model and elevation						
(Intercept)	1.010	0.135	0.736	1.014	1.265	1.023
Easting	-4.127	1.762	-7.596	-4.128	-0.661	-4.130
Northing	-0.309	0.245	-0.797	-0.307	0.171	-0.304
Elevation	-1.048	0.227	-1.497	-1.047	-0.603	-1.045
Fixed effects model						
(Intercept)	2.053	0.212	1.656	2.045	2.491	2.031
Easting	-4.080	1.336	-6.730	-4.071	-1.481	-4.054
Northing	-0.200	0.187	-0.565	-0.200	0.167	-0.201
Precipitation	0.176	0.231	-0.272	0.174	0.634	0.170
Snow	-0.168	0.190	-0.546	-0.166	0.200	-0.162
flat	1.091	1.084	-0.729	0.979	3.504	0.738
summit	0.071	1.079	-1.768	-0.033	2.456	-0.252
ridge	0.702	0.481	-0.184	0.681	1.707	0.639
shoulder	0.000	31.623	-62.086	-0.001	62.034	0.000
spur	1.204	0.358	0.519	1.198	1.927	1.186
hollow	0.405	0.463	-0.448	0.385	1.371	0.345
footslope	2.225	1.922	-0.851	1.970	6.613	1.376
valley	-0.228	0.555	-1.232	-0.259	0.948	-0.321
depression	0.000	31.623	-62.086	-0.001	62.034	0.000
Elevation	-0.869	0.202	-1.279	-0.865	-0.486	-0.855
Fixed Effects Parasite Survival Model						
(Intercept)	2.550	0.216	2.148	2.542	2.999	2.526
Precipitation	0.321	0.194	-0.056	0.320	0.706	0.317
Snow	-0.433	0.190	-0.807	-0.433	-0.061	-0.432
flat	0.830	1.129	-1.056	0.710	3.350	0.449
summit	-0.956	1.088	-2.784	-1.069	1.465	-1.311
ridge	0.445	0.494	-0.460	0.422	1.482	0.374
shoulder	0.000	31.623	-62.086	-0.001	62.034	0.000
spur	1.143	0.369	0.439	1.135	1.888	1.121
hollow	0.868	0.474	0.000	0.845	1.861	0.800

Table 6: Fixed effect parameter estimates and distribution for *P. tenuis (continued)*

variable	mean	sd	0.025quant	0.5quant	0.975quant	mode
footslope	2.610	1.996	-0.566	2.339	7.175	1.704
valley	-0.390	0.563	-1.399	-0.425	0.813	-0.496
depression	0.000	31.623	-62.086	-0.001	62.034	0.000

Table 7: Random effect parameter estimates and distribution for *F. magna*

variable	mean	sd	0.025quant	0.5quant	0.975quant	mode
Null Model						
Nbinomial disp. par.	0.122	0.008	0.106	0.121	0.139	0.121
Full model						
Nbinomial disp. par.	0.170	0.015	0.142	0.170	0.201	0.169
Range for i	675.719	393.696	174.797	591.888	1689.579	430.606
Stdev for i	3.829	1.941	1.456	3.371	8.845	2.677
Two-scale spatial model						
Nbinomial disp. par.	0.157	0.013	0.131	0.157	0.183	0.158
Range for i	8822.205	6098.497	1930.233	7312.316	24616.287	4794.180
Stdev for i	1.365	0.285	0.827	1.364	1.924	1.379
Two-scale spatial model and elevation						
Nbinomial disp. par.	0.154	0.014	0.128	0.153	0.182	0.153
Range for i	762.009	771.156	106.883	535.157	2785.808	271.417
Stdev for i	4.462	3.808	0.754	3.401	14.466	1.923
Fixed effects model						
Nbinomial disp. par.	0.133	0.009	0.115	0.133	0.152	0.132
Fixed Effects Parasite Survival Model						
Nbinomial disp. par.	0.131	0.009	0.114	0.131	0.150	0.130

Table 8: Random effect parameter estimates and distribution for *P. tenuis*

variable	mean	sd	0.025quant	0.5quant	0.975quant	mode
Null Model						
Nbinomial disp. par.	0.081	0.006	0.070	0.081	0.093	0.081
Full model						
Nbinomial disp. par.	0.111	0.010	0.092	0.110	0.132	0.110
Range for i	508.951	311.124	160.420	429.334	1343.793	318.308
Stdev for i	5.303	2.658	1.678	4.797	12.159	3.833
Two-scale spatial model						
Nbinomial disp. par.	0.111	0.010	0.093	0.111	0.131	0.110
Range for i	8705.474	4450.205	2871.060	7799.328	19903.368	6169.912
Stdev for i	1.892	0.397	1.297	1.827	2.838	1.688
Two-scale spatial model and elevation						
Nbinomial disp. par.	0.106	0.009	0.089	0.106	0.126	0.106
Range for i	585.296	394.178	169.375	478.445	1659.697	342.033
Stdev for i	4.439	2.257	1.315	4.029	9.984	3.166
Fixed effects model						

Table 8: Random effect parameter estimates and distribution for *P. tenuis (continued)*

variable	mean	sd	0.025quant	0.5quant	0.975quant	mode
Nbinomial disp. par.	0.093	0.007	0.080	0.092	0.107	0.092
Fixed Effects Parasite Survival Model						
Nbinomial disp. par.	0.084	0.006	0.073	0.084	0.097	0.084